Research Square

Preprints are preliminary reports that have not undergone peer review.
They should not be considered conclusive, used to inform clinical practice,
or referenced by the media as validated information.

Data-driven FDG-PET subtypes of Alzheimer's disease-related neurodegeneration

Fedor Levin
German Centre for Neurodegenerative Diseases: Deutsches Zentrum fur Neurodegenerative Erkrankungen
https://orcid.org/0000-0002-0518-1715
Daniel Ferreira
Karolinska Institutet
Catharina Lange
Charite Universitatsmedizin Berlin
Martin Dyrba
German Centre for Neurodegenerative Diseases: Deutsches Zentrum fur Neurodegenerative Erkrankungen
Eric Westman
Karolinska Institutet
Ralph Buchert
University Medical Center Hamburg-Eppendorf: Universitatsklinikum Hamburg-Eppendorf
Stefan Teipel
German Centre for Neurodegenerative Diseases: Deutsches Zentrum fur Neurodegenerative Erkrankungen
Michel Grothe (mgrothe@us.es)
Campus Hospital Universitario Virgen del Rocío https://orcid.org/0000-0003-2600-9022

Research

Keywords: Alzheimer's disease, subtypes, mild cognitive impairment, prodromal, FDG-PET, hypometabolism

Posted Date: November 5th, 2020

DOI: https://doi.org/10.21203/rs.3.rs-100844/v1

License: This work is licensed under a Creative Commons Attribution 4.0 International License. Read Full License

Version of Record: A version of this preprint was published on February 19th, 2021. See the published version at https://doi.org/10.1186/s13195-021-00785-9.

Abstract

Background

Previous research has described distinct subtypes of Alzheimer's disease (AD) based on differences in regional patterns of brain atrophy on MRI. We conducted a data-driven exploration of distinct AD neurodegeneration subtypes using FDG-PET as a sensitive molecular imaging marker of neurodegenerative processes.

Methods

Hierarchical clustering of voxel-wise FDG-PET data from 177 amyloid-positive patients with AD dementia enrolled in the Alzheimer's Disease Neuroimaging Initiative (ADNI) was used to identify distinct hypometabolic subtypes of AD, which were then further characterized with respect to clinical and biomarker characteristics. We then classified FDG-PET scans of 217 amyloid-positive patients with mild cognitive impairment ('prodromal AD') according to the identified subtypes and studied their domain-specific cognitive trajectories and progression to dementia over a follow-up interval of up to 72 months.

Results

Three main hypometabolic subtypes were identified: (i) "typical" (48.6%), showing a classic posterior temporo-parietal hypometabolic pattern, (ii) "limbic-predominant" (44.6%), characterized by old age and a memory-predominant cognitive profile, and (iii) a relatively rare "cortical-predominant" subtype (6.8%) characterized by younger age and more severe executive dysfunction. Subtypes classified in the prodromal AD sample demonstrated similar subtype characteristics as in the AD dementia sample and further showed differential courses of cognitive decline.

Conclusions

These findings complement recent research efforts on MRI-based identification of distinct AD atrophy subtypes and may provide a potentially more sensitive molecular imaging tool for early detection and characterization of AD-related neurodegeneration variants at prodromal disease stages.

Introduction

Previous research has demonstrated heterogeneity in Alzheimer's disease (AD) which is linked to distinct neuropathological subtypes of AD characterized by limbic-predominant, hippocampal-sparing, or rather balanced ("typical") spatial distributions of neurofibrillary tangle pathology (1). Analysis of ante-mortem structural MRI data demonstrated that neuropathologically-defined AD subtypes also show characteristic in-vivo patterns of regional brain atrophy (2). Recent research has used clustering methods on structural MRI data to identify similar regional atrophy subtypes in AD in a data-driven manner (3). Interestingly, these atrophy subtypes could already be detected in patients with prodromal AD (i.e. amyloid-beta [Aβ] positive patients with mild cognitive impairment [MCI]), who showed similar biomarker characteristics as the subtypes identified in patients with AD dementia and were associated with differential clinical trajectories (4, 5).

In addition to volumetric information from structural MRI, hypometabolism in FDG-PET is a well-established imaging marker of neurodegeneration as recognized by the recently revised research criteria for AD (6). FDG-PET

may indicate a decrease in cerebral glucose metabolism that occurs prior to the macroscopic atrophy detectable with MRI, rendering the technique potentially more sensitive to early neurodegenerative processes (7-9). Dementia-specific FDG-PET patterns are already widely used for aiding early and differential dementia diagnosis (10-13). While previous hypothesis-driven studies have also reported differential hypometabolic FDG-PET patterns among AD dementia patients (10, 14, 15), to our knowledge, FDG-PET has not yet been used for identifying neurodegeneration subtypes of AD in a data-driven manner.

In the current study we aimed to investigate and characterize hypometabolic subtypes in patients with AD by applying an established hierarchical clustering approach to a large dataset of FDG-PET scans from patients with biomarker-confirmed AD enrolled in the Alzheimer's Disease Neuroimaging Initiative (ADNI). We also used the identified subtypes for classification of an independent ADNI sample of patients with prodromal AD (Aβ-positive patients with MCI) who were clinically followed for up to 72 months.

Methods

Participants

We included data from 179 cognitively normal (CN) participants (58 Aβ-positive), 177 Aβ-positive patients with a clinical diagnosis of AD dementia, and 217 Aβ-positive patients with MCI (i.e. prodromal AD) from the ADNI-1, ADNI-GO/2 and ADNI-3 cohorts (adni.loni.usc.edu). Detailed inclusion criteria for the different diagnostic categories have been described in detail before (16) and are available on the ADNI website (http://adni.loni.usc.edu/methods/documents/). Evidence of Aβ pathology was based on AV45-PET or, in case this measure was not available, on CSF Aβ levels (see below for details). The ADNI is a longitudinal multicentre study aimed at investigating whether neuroimaging methods such as MRI and PET, together with genetic, clinical and neuropsychological measures can be used to characterize progression of MCI and AD. The ADNI was launched in 2003 as a public-private partnership, led by Principal Investigator Michael W. Weiner, MD.

Neuropsychological Test Scores

Cognitive performance in the ADNI is assessed using neuropsychological test batteries covering various cognitive domains. We used previously established composite cognitive scores for memory (ADNI-MEM) and for executive function (ADNI-EF) (17, 18). Additionally, we used the score on the Clock Drawing test as a measure of visuospatial function, and the Boston Naming Test score as a measure of language function(4). Mini Mental State Examination (MMSE) scores were used for characterizing global cognitive impairment. We also calculated the difference between the ADNI-MEM and the ADNI-EF composite scores (ADNI-DIFF) to characterize differential decline in these two domains. Positive values in this variable thus represent a more pronounced executive impairment compared to the memory deficit, and vice versa for negative values.

Longitudinal analysis

We analysed longitudinal changes in cognitive functions of the prodromal AD subtypes for participants with available follow-up data (n = 200). We used longitudinal measures of ADNI-MEM, ADNI-EF, Clock Drawing test and the Boston Naming Test. Additionally, longitudinal Clinical Dementia Rating (CDR) scores were used as a criterion indicating progression from prodromal (CDR = 0.5) to clinically manifest AD dementia (CDR $\geq$ 1). Mean follow-up

period was 44 months (range 12-72 months), and 72.5% of participants had at least 36 months of follow-up available.

Biomarkers

Measures of cortex-to-whole cerebellum AV45 standard uptake value ratios (SUVR) have been calculated by the ADNI PET core (Jagust Lab, UC Berkeley) and were downloaded from the ADNI server. We selected Aβ positive patients with AD or MCI if their AV45 SUVR values were greater than or equal to the recommended threshold of 1.11 (19).

ADNI CSF values in the current study were derived from electrochemiluminescence immunoassays for Aβ (1-42), phospho-Tau (181P), and total-Tau on an automated Elecsys cobas e 601 instrument[1]. We included participants who had CSF Aβ values lower than the threshold of 880 pg/ml proposed by Hansson et al. (20).

APOE genotype was determined using DNA extracted from a 3-mL aliquot of EDTA blood samples by Cogenics (21). Genotype information was coded in a binary *APOE* ε4 variable indicating the presence of at least one *APOE* ε4 allele.

Structural MRI images were used to derive hippocampal and cortical volume measures. MRI images in ADNI are acquired at multiple sites using scanner-specific T1-weighted sagittal 3D MPRAGE sequences and undergo standardized image pre-processing steps to improve uniformity across the scanners (http://adni.loni.usc.edu/methods/documents/). We extracted regional grey matter volumes from these scans using a previously described automated volumetry approach implemented in statistical parametric mapping software (SPM8, Wellcome Trust Center for Neuroimaging) and the VBM8-toolbox (22, 23). Briefly, this involves automated tissue class segmentation and high-dimensional spatial normalization to an aging/AD-specific reference template. Spatially normalized grey matter (GM) maps were visually inspected for segmentation and normalization accuracy, and voxel values were modulated for volumetric changes introduced by the high-dimensional normalization, so that the total GM volume present before warping was preserved. Hippocampal (HV) and regional cortical grey matter volumes were extracted from these scans using regions-of-interest defined in the Harvard-Oxford anatomical atlas (24). Individual volumes were divided by the total intracranial volume (TIV), calculated as the sum of total volumes of all tissue segments. In analogy to previous MRI-based subtyping studies (2, 25), cortical grey matter volumes were extracted from selected frontal, temporal, and parietal association areas (see Supplementary table 1), summed into a measure of bilateral cortical total volume (CTV), and further used to calculate the hippocampal to cortical volume ratio (HV:CTV).

Finally, we included white matter hyperintensity (WMH) volume as a measure of small vessel vascular disease burden. These values have been calculated by the ADNI MRI core and were downloaded from the ADNI server. In ADNI-1 data WMH values were obtained via analysis of the proton density (PD), T1 and T2 MRIs (26). In ADNI-GO/2, a fluid-attenuated inversion recovery (FLAIR) MRI sequence was used to calculate WMH volumes (27). In the present study we pooled available WMH measures (4) and controlled statistical analyses of this variable for different segmentation methods using a dummy-coded confound variable.

FDG-PET data acquisition and preprocessing

FDG-PET data were retrieved in a pre-processed form from the ADNI server. FDG-PET images were obtained on multiple scanners with protocols specific to platforms. Dynamic 3D scans of six 5-minute frames were acquired 30-60 minutes after injections of 185 MBq of ^{18}F-FDG. All original ADNI FDG-PET scans underwent standardized image pre-processing steps to improve uniformity across the scanners. Detailed information on FDG-PET acquisition and pre-processing is available on the ADNI website (http://adni.loni.usc.edu/methods/documents/). For the present study, FDG-PET images were further spatially normalized to a customized FDG-PET standard space template and smoothed with a Gaussian smoothing kernel of 8 mm full-width at half maximum (FWHM) using SPM8 (28).

Hierarchical clustering

The patients with AD dementia were classified into hypometabolic subtypes using agglomerative hierarchical clustering of voxel-wise FDG-PET data with Ward's linkage as implemented in MATLAB software (29, 30). Individual FDG-PET profiles were scaled to their global mean prior to clustering analysis so that clustering relies on differences in regional FDG-PET patterns rather than on global signal differences across patients. In the clustering procedure, the algorithm progressively combines closest voxel-wise FDG-PET profiles of the participants into larger clusters, as well as most similar clusters with each other. Output of the algorithm is a hierarchical dendrogram in which the level of branching indicates the degree of dissimilarity between the clusters. The optimal number of separable clusters in the data was evaluated using standard performance measures for clustering solutions including the Davies-Bouldin criterion (31) and the silhouette criterion (32).

To visualize patterns of hypometabolism in the identified subtypes, we conducted voxel-wise two-sample t-tests between FDG-PET images from each of the subtypes and the CN group, using age, gender, and years of education as covariates. Images were scaled to the average signal in a pons reference region prior to analysis. An explicit grey matter mask was applied to the images and obtained t values were converted into Cohen's d effect size values.

Classification of patients with prodromal AD

We classified FDG-PET scans of patients with prodromal AD according to the identified AD subtypes using a fully automated classification procedure. For that, we first screened patients for evidence of regional hypometabolism by assessing whether at least one of the 48 bilateral cortical areas defined in the Harvard-Oxford atlas had an FDG-PET signal (scaled to pons) of at least one standard deviation below the mean of the control group. Participants with no such regions were classified into a "no hypometabolism" subtype (10, 11). The remaining patients with prodromal AD were classified into one of the subtypes identified in the AD dementia group based on the smallest Euclidean distance between the individual patient's voxel-wise FDG-PET profile (scaled to global values) and the mean FDG-PET profile of each of the AD dementia subtypes (4).

Statistical analysis

Statistical analyses were conducted using RStudio and R version 3.5.2 with a statistical significance threshold of $P < 0.05$ (two-tailed). Chi-squared tests with post-hoc pairwise proportion tests were used to compare gender

compositions of subtypes and frequencies of the *APOE* ε4 genotype. For this and other post-hoc tests comparing subtypes we used the false discovery rate (FDR) correction (33) as implemented in R. Age and years of education were compared across subtypes using ANOVA. Differences in cognitive measures and biomarkers across the subtypes were tested with ANCOVA using age, gender, and education as covariates (34, 35).

For patients with prodromal AD with available clinical follow-up data, we also conducted Cox proportional hazards regression analyses for analysing differential risks of progression to dementia across FDG-PET defined subtypes. Progression to dementia was operationalized as a change in CDR score from 0.5 to ≥ 1. Models included age, gender, and education as covariates. Participants were censored if they did not progress to dementia before the last available follow-up CDR score.

In addition, linear mixed effects regression models were used to assess differences in domain-specific longitudinal changes in memory, executive function, visuospatial function or language function. Models included time of follow-up measured in months from baseline, a factor variable indicating subtype, and an interaction term for time by subtype as independent variables. The estimates for interactions between subtype and time indicated whether subtypes had differential cognitive trajectories over time. Age, gender, and education were included as covariates. Regression models included random intercepts and random slopes for participants; t-tests used Satterthwaite approximations for degrees of freedom.

[1] The Elecsys β-Amyloid(1-42) CSF immunoassay in use is not a commercially available IVD assay. It is an assay that is currently under development and for investigational use only. The measuring range of assay is 200 (lower technical limit) – 1700 pg/mL (upper technical limit). The performance of the assay beyond the upper technical limit has not been formally established. Therefore, use of values above the upper technical limit, which are provided based on an extrapolation of the calibration curve, is restricted to exploratory research purposes and is excluded for clinical decision making or for the derivation of medical decision points.

Results

Identification of hypometabolic subtypes in patients with AD dementia

We used objective criteria for evaluating optimal clustering solutions to select the level of cutoff for the hierarchical clustering dendrogram supported by the data. The Davies-Bouldin criterion favoured solutions with three or five clusters, whereas the silhouette criterion favoured three clusters (see Supplementary figure 1). Therefore, we chose the clustering solution with three clusters (see results for solutions with higher cluster numbers in the Supplementary figure 2). Cluster-1 included 44.6% of the patients and showed a predominantly limbic hypometabolic profile with most pronounced hypometabolism in the medial temporal lobe, which extended to the posterior cingulate cortex, lateral temporo-parietal areas, and also large areas of the ventromedial and lateral frontal lobe (Figure 1; henceforth referred to as the “limbic-predominant” subtype). Cluster-2 included 48.6% of the patients and corresponded to a more AD-typical pattern of marked posterior temporo-parietal hypometabolism with additional, albeit less pronounced, involvement of the medial temporal lobe (henceforth referred to as the “typical” subtype). Cluster-3 included 6.8% of the patients and showed a pattern of temporo-parietal cortical hypometabolism similar to that of cluster-2, but with more extensive involvement of the frontal

lobe and largely spared metabolism in the medial temporal lobe (henceforth referred to as the “cortical-predominant” subtype).

Characterization of the hypometabolic subtypes in patients with AD dementia

Demographic, clinical, and biomarker characteristics of the three AD subtypes are listed in Table 1. The “limbic-predominant” hypometabolic subtype was the oldest with an average age of 75.4 years and the “cortical-predominant” subtype the youngest with an average age of 68.0 years. The “limbic-predominant” subtype generally showed the least pronounced impairments in neuropsychological testing and was characterized by a memory-predominant cognitive profile, whereas in the “typical” and especially the “cortical-predominant” subtype the impairment in executive functions exceeded the mnestic deficit. Reflecting the subtype-defining hypometabolic patterns, hippocampal volume was lowest in the “limbic-predominant” subtype and highest in the “cortical-predominant” subtype, whereas cortical volumes showed the opposite behaviour. The resulting HV:CTV ratio was significantly higher for the “cortical-predominant” subtype in comparison to the two other subtypes. The “cortical-predominant” subtype also had a strikingly lower percentage of *APOE* ε4 carriers compared to the other two subtypes, although this difference did not reach statistical significance. No differences were observed between the subtypes with regard to gender distribution, years of education, molecular biomarkers of Aβ and tau pathology burden, or WMH volume (Table 1).

Characterization and longitudinal trajectories of the hypometabolic subtypes in patients with prodromal AD

About a quarter (26.3%) of the prodromal AD cohort did not show any evidence of regional hypometabolism and was thus classified as “no hypometabolism” subtype. Among the other patients with prodromal AD, 49.8% were classified into the “limbic-predominant” subtype, 22.6% into the “typical” subtype, and only three participants (1.4%) were classified into the “cortical-predominant” subtype, which was thus omitted from further analyses. Hypometabolic patterns of the classified subtypes in the prodromal AD cohort showed a strong spatial resemblance with the subtype-defining patterns in the AD dementia cohort (Figure 2), thus corroborating the validity of the automated classification procedure. Demographic, clinical, and biomarker characteristics of the subtypes are summarized in Table 2.

The “limbic-predominant” subtype was again characterized by a significantly higher age compared to the other subtypes. The “no hypometabolism” subtype was the youngest and also had a higher proportion of females. Despite no pairwise differences in MMSE scores, the “no hypometabolism” subtype also showed significantly better memory and executive function performance than the “typical” and the “limbic-predominant” subtypes. Although we selected only Aβ-positive patients, the “no hypometabolism” subtype showed a significantly lower Aβ burden on both PET and CSF measures. Additionally, the “no hypometabolism” subtype had significantly higher hippocampal and cortical volumes compared to the “limbic-predominant” and the “typical” subtypes.

Longitudinal analyses showed that the “no hypometabolism” subtype was at the lowest risk of progression to dementia (vs “limbic-predominant”: HR: 4.82, $P < 0.001$; vs “typical”: HR: 5.99, $P < 0.001$), but there were no differences between the “typical” and “limbic-predominant” subtypes ($P = 0.456$; Figure 3, see Supplementary table 2 for full model stats).

The “no hypometabolism” subtype also showed a significantly slower decline in all four cognitive domains, compared to the “typical” subtype (for all comparisons, $P < 0.05$), as well as a significantly slower decline in memory, executive, and language functions compared to the “limbic-predominant” subtype (for all comparisons, $P < 0.01$; Figure 4, see Supplementary table 3 for full model stats). Interestingly, the “typical” and “limbic-predominant” subtypes showed a similar decrease in memory function over time, but the “typical” subtype showed a significantly faster decline in executive ($t = -2.247$, $P = 0.026$) and visuospatial functions ($t = -2.235$, $P = 0.027$) than the “limbic-predominant” subtype (see Supplementary table 4 for full model stats).

Discussion

In the current study we identified three distinct subtypes of hypometabolic patterns on FDG-PET scans among patients with AD dementia and characterized them with respect to clinical and biomarker profiles. We further used the identified subtypes to stratify an independent sample of patients with prodromal AD and studied subtype-specific clinical trajectories over up to 72 months of follow-up. The subtypes differed in various demographic characteristics, biomarker levels, and cognitive performance at baseline. Moreover, in the prodromal AD cohort the subtypes were associated with differential trajectories of cognitive decline.

The “typical” subtype included the largest portion of AD dementia cases and was characterized by a typical posterior temporo-parietal pattern of hypometabolism that is commonly linked to AD (13, 36). The “limbic-predominant” subtype had most pronounced hypometabolism in the hippocampus and related medial temporal structures which showed similarities to the MRI-defined medial temporal-predominant atrophy subtypes (4, 30, 37, 38). However, the “limbic-predominant” subtype in the current study also showed hypometabolism in more widespread limbic areas and the frontal lobe. A previous study examining FDG-PET patterns in MRI-defined atrophy subtypes also reported pronounced frontal hypometabolism in the medial temporal-predominant AD atrophy subtype (38). A wider extent of limbic hypometabolism extending into the frontal lobe despite a rather restricted medial temporal atrophy pattern, could reflect remote effects of atrophy on dysfunction in distant but functionally interconnected brain areas (16, 39-41).

Similarly to previous findings on the MRI-defined medial temporal-predominant atrophy subtype (4, 37), the “limbic-predominant” hypometabolic subtype in the current study was associated with older age and could possibly reflect the effects of comorbid age-related pathologies. For example, Zhang et al. (5) considered that the temporal factor described in their study could be linked to comorbid TDP-43 pathology. Indeed, the hypometabolic pattern of the “limbic-predominant” subtype identified in the present study shows a striking resemblance with a recently described FDG-PET pattern of pathologically confirmed patients with AD dementia with comorbid TDP-43 pathology and hippocampal sclerosis (42). Other studies suggested that the medial-temporal subtype could be additionally affected by small vessel disease (4, 43), which would coincide with the numerically highest WMH volume in the “limbic-predominant” subtype in our study. However, this difference did not reach statistical significance in our analysis.

The hypometabolic pattern of the “cortical-predominant” subtype was similar to that of the “typical” subtype, but with more extensive involvement of the frontal lobe and largely normal metabolism in the medial temporal lobe. This subtype showed particularly pronounced executive function impairment in addition to the memory deficit. Previously, studies by Collette et al. (14) and Mosconi et al. (10) have also described marked frontal hypometabolism in subsets of patients with AD. On the other side, Ossenkoppele et al. (44) described an

autopsy/biomarker-confirmed dysexecutive AD variant, which shows markedly more pronounced impairment in executive function relative to the memory deficit, and is characterized by early onset of AD and a relatively low *APOE* ε4 frequency. Similarly, the “cortical-predominant” subtype in the current study also showed the youngest age, lowest executive function performance, and lowest percentage of *APOE* ε4 carriers among AD subtypes. However, due to the low number of patients in this group, current findings on this subtype require further corroboration.

Additionally, we observed a difference between subtypes in the HV:CTV ratio. Specifically, it was the highest for the cortical-predominant subtype, intermediate for the typical, and numerically the lowest for the limbic-predominant subtype. The pattern of differences in HV:CTV ratio between FDG-PET subtypes in the current study is comparable to previous findings on AD subtypes based on neuropathological data or MRI-based atrophy patterns. The study by Whitwell et al. (2) examined AD subtypes based on neuropathological examination of distribution of neurofibrillary tangle counts. The ratio between hippocampal and cortical volumes measured on ante-mortem MRI allowed for the best discrimination between these subtypes. In their study, similarly to our results, the typical subtype showed a higher HV:CTV ratio than the limbic-predominant subtype, whereas the hippocampal sparing subtype had the highest value. Furthermore, in the study by Risacher et al. (25), three AD subtypes - hippocampal sparing, limbic predominant and typical AD - were defined based on the HV:CTV ratio. Across these subtypes, a higher HV:CTV ratio was also quantitatively associated with a more pronounced dysexecutive profile, similarly to the differences observed for the ADNI-EF and ADNI-DIFF variables between the subtypes in the current study. Therefore, the HV:CTV ratio measured in the current subtypes provides a link between our findings on hypometabolism subtypes and previously characterized AD subtypes based on neuropathological data or MRI-based atrophy patterns. However, there were also differences between the observed hypometabolism subtypes and previously reported atrophy patterns on MRI, such as the aforementioned more extensive involvement of the temporal and frontal areas in the “limbic-predominant” hypometabolism subtype, which might be attributed to the different structural and functional substrates of the respective imaging methods.

Before classifying the independent cohort of patients with prodromal AD based on their similarity to the AD subtypes, we identified a group of patients who showed no indication of hypometabolism in cortical regions and characterized it as a distinct “no hypometabolism” subtype. The “no hypometabolism” subtype had the least pathologic biomarker measures, the least cognitive impairment, and the lowest risk of progressing to dementia. Previous studies using visual classification of FDG-PET scans had also described subsets of patients with MCI without evidence of regional hypometabolism (10, 11). In the study by Cerami et al. (11), 31% of participants with MCI showed normal brain metabolism, although the large majority of these also had a negative amyloid biomarker finding. However, MRI-based subtyping studies have also consistently identified subsets of patients with AD dementia with no or only minimal atrophy, and this subtype was particularly prevalent among patients with prodromal AD (4, 37, 45). Interestingly, in our study we observed a similar “minimal” hypometabolism subtype in the AD dementia group when using a higher clustering solution (see Supplementary figure 2). However, since we established the best distinguishable AD subtypes using an objective hierarchical clustering cutoff as suggested by the Davies-Bouldin and the silhouette criteria, we did not further characterize this “minimal” subtype in our study. Nevertheless, our findings underline the importance of accounting for the considerably sized subgroup of patients with prodromal AD without evidence of regional hypometabolism when characterizing heterogeneity of hypometabolism patterns in this population.

Patients with prodromal AD classified into the “limbic-predominant” and the “typical” subtypes showed patterns of differences in demographic, cognitive, and biomarker characteristics similar to those observed in the respective AD dementia subtypes. The “limbic-predominant” subtype had older age, numerically higher WMH volume and the most severe degree of hippocampus atrophy. Thus, current results confirm previous findings that the heterogeneity evident in patients with AD dementia can also be observed at the prodromal stage of the disease. Only three participants with prodromal AD were classified into the “cortical-predominant” subtype. One potential explanation for this low prevalence could be that this hypometabolic subtype is characterized by more pronounced executive function deficits than memory deficits from its prodromal stage on, so that these patients would be underrepresented in an MCI cohort screened for memory deficits such as the ADNI cohort.

In longitudinal analyses of clinical follow-up data, the “typical” subtype demonstrated a quicker decline of executive function and visuospatial function as compared to the “limbic-predominant” subtype. This finding is notable, because these subsets of patients with prodromal AD did not show significant differences in these functions at baseline. This indicates that subtype classification of FDG-PET patterns may provide additional information for predicting future cognitive decline that is not contained in neuropsychological assessments.

One conceptual strength of the current study is that we only included patients with biomarker evidence of Aβ pathology. Moreover, we used the identified hypometabolism subtypes in patients with AD dementia to classify an independent dataset of Aβ-positive patients with MCI and assess clinical and biomarker characteristics of these subtypes at a prodromal disease stage. However, in the prodromal AD group, the “no hypometabolism” subtype demonstrated relatively low Aβ levels. Therefore, it is possible that some patients in this group could have only incidental Aβ-pathology.

Limitations

As with other unsupervised subtyping studies, a principal limitation of the current study is that the employed clustering methodology cannot naturally distinguish between subtypes and different disease stages. For example, the “no hypometabolism” subtype of the prodromal AD group could theoretically represent an earlier stage of any of the other hypometabolic subtypes. Similarly, the “cortical-predominant” subtype could potentially also represent a more advanced stage of the “typical” subtype in the AD group. While the current methodology cannot directly disprove this alternative explanation we aimed to mitigate the effect of differing disease stages by normalizing the individual FDG-PET profiles to their global signal before clustering, so that the cluster assignations were primarily driven by relative regional metabolic differences instead of global differences accompanying disease progression. Moreover, we note that the identified subtypes show several biomarker characteristics that would not be consistent with an interpretation of successive disease stages, such as for example numerically lower hippocampal volumes and higher *APOE* ε4 prevalence in the “typical” compared to the “cortical-predominant” subtype. The contribution of disease stage to observed subtype phenotypes has been addressed in a recent MRI-based subtyping study by Young et al. (46), which proposed an analytical approach combining clustering with event-based modelling to assess subtypes and their respective stage progressions at the same time. However, this approach still relies on extrapolations from cross-sectional data. Future research on neurodegeneration subtypes in AD will benefit from longitudinal imaging assessments allowing to directly characterize disease progression within subtypes and to determine the possibility of conversion between them.

Conclusion

In the current study we used a systematic data-driven approach for characterizing differential neurodegeneration subtypes in AD as reflected by hypometabolism patterns on FDG-PET. The hypometabolic subtypes were associated with differential clinical and biomarker profiles, as well as with differences in clinical trajectories over time. These findings complement recent research efforts on characterizing distinct atrophy subtypes in AD using structural MRI data. Due to the reportedly higher sensitivity of FDG-PET for early neurodegenerative changes, the described hypometabolic subtypes may provide a sensitive tool for early detection and characterization of AD-related neurodegeneration variants at prodromal disease stages, which may have important implications for improving timely and differentiated prognosis in non-demented individuals with biomarker evidence of AD.

Abbreviations

AD: Alzheimer's disease; ADNI: Alzheimer's Disease Neuroimaging Initiative; ADNI-DIFF: difference between ADNI-MEM and ADNI-EF; ADNI-EF: ADNI composite cognitive score for executive function; ADNI-MEM: ADNI composite cognitive score for memory function; APOE: Apolipoprotein E; Aβ: Beta-amyloid; CDR: Clinical Dementia Rating; CN: Cognitively normal; CSF: Cerebrospinal fluid; CTV: Cortical composite grey matter volume scaled to total intracranial volume; FDG: Fluorodeoxyglucose; FDR: False discovery rate; GM: Grey matter; HV: Hippocampal grey matter volume scaled to total intracranial volume; MCI: Mild cognitive impairment; MMSE: Mini Mental State Examination; MRI: Magnetic resonance imaging; PET: Positron emission tomography; SUVR: Standard uptake value ratio; TIV: Total intracranial volume; WM: White matter; WMH: White matter hyperintensity volume.

Declarations

Authors' contributions

FL, SJT and MJG designed and conceptualized the study; FL, SJT, MJG and MD analyzed the data; FL, SJT, MJG and DF drafted the manuscript for intellectual content; all authors interpreted the data, revised the manuscript for intellectual content, read and approved the final manuscript.

Acknowledgements

The authors would like to thank the Swedish Research Council (VR).

Funding

Michel J. Grothe is supported by the "Miguel Servet" program [CP19/00031] of the Spanish Instituto de Salud Carlos III (ISCIII-FEDER).

Data collection and sharing for this project was funded by the Alzheimer's Disease Neuroimaging Initiative (ADNI) (National Institutes of Health Grant U01 AG024904) and DOD ADNI (Department of Defense award number W81XWH-12-2-0012). ADNI is funded by the National Institute on Aging, the National Institute of Biomedical Imaging and Bioengineering, and through generous contributions from the following: AbbVie, Alzheimer's Association; Alzheimer's Drug Discovery Foundation; Araclon Biotech; BioClinica, Inc.; Biogen; Bristol-Myers Squibb Company; CereSpir, Inc.; Cogstate; Eisai Inc.; Elan Pharmaceuticals, Inc.; Eli Lilly and Company; EuroImmun; F. Hoffmann-La Roche Ltd and its affiliated company Genentech, Inc.; Fujirebio; GE Healthcare; IXICO Ltd.; Janssen Alzheimer Immunotherapy Research & Development, LLC.; Johnson & Johnson Pharmaceutical Research & Development LLC.; Lumosity; Lundbeck; Merck & Co., Inc.; Meso Scale Diagnostics, LLC.; NeuroRx

Research; Neurotrack Technologies; Novartis Pharmaceuticals Corporation; Pfizer Inc.; Piramal Imaging; Servier; Takeda Pharmaceutical Company; and Transition Therapeutics. The Canadian Institutes of Health Research is providing funds to support ADNI clinical sites in Canada. Private sector contributions are facilitated by the Foundation for the National Institutes of Health (www.fnih.org). The grantee organization is the Northern California Institute for Research and Education, and the study is coordinated by the Alzheimer's Therapeutic Research Institute at the University of Southern California. ADNI data are disseminated by the Laboratory for Neuro Imaging at the University of Southern California.

Availability of data and materials

Data analyzed in this study were acquired from the Alzheimer's Disease Neuroimaging Initiative (ADNI) database (http://adni.loni.usc.edu). ADNI data are shared in a de-identified form and without embargo subject to a review of a data use application by the ADNI Data Sharing and Publications Committee. For further information please refer to the ADNI website (http://adni.loni.usc.edu/data-samples/access-data/).

Ethics approval and consent to participate

Data collection and sharing in ADNI was approved by the Institutional Review Board of each participating institution. All procedures involving human participants were in accordance with the ethical standards of the 1964 Helsinki declaration and its later amendments. Written informed consent was obtained from all ADNI participants and/or authorized representatives before any protocol-specific procedures were carried out.

Consent for publication

Not applicable.

Competing interests

SJT participated in scientific advisory boards of Roche Pharma AG and MSD and received lecture fees from Roche and MSD. MJG, FL, CL, MD, EW and RB have no disclosures to report.

References

1. Murray ME, Graff-Radford NR, Ross OA, Petersen RC, Duara R, Dickson DW. Neuropathologically defined subtypes of Alzheimer's disease with distinct clinical characteristics: a retrospective study. The Lancet Neurology. 2011;10(9):785-96.
2. Whitwell JL, Dickson DW, Murray ME, Weigand SD, Tosakulwong N, Senjem ML, et al. Neuroimaging correlates of pathologically defined subtypes of Alzheimer's disease: a case-control study. The Lancet Neurology. 2012;11(10):868-77.
3. Habes M, Grothe MJ, Tunc B, McMillan C, Wolk DA, Davatzikos C. Disentangling Heterogeneity in Alzheimer's Disease and Related Dementias Using Data-Driven Methods. Biological psychiatry. 2020.
4. Ten Kate M, Dicks E, Visser PJ, van der Flier WM, Teunissen CE, Barkhof F, et al. Atrophy subtypes in prodromal Alzheimer's disease are associated with cognitive decline. Brain. 2018;141(12):3443-56.
5. Zhang X, Mormino EC, Sun N, Sperling RA, Sabuncu MR, Yeo BT, et al. Bayesian model reveals latent atrophy factors with dissociable cognitive trajectories in Alzheimer's disease. Proc Natl Acad Sci U S A.

2016;113(42):E6535-E44.
6. NIA-AA Research Framework: Toward a biological definition of Alzheimer's disease, (2018).
7. Kljajevic V, Grothe MJ, Ewers M, Teipel S, Alzheimer's Disease Neuroimaging I. Distinct pattern of hypometabolism and atrophy in preclinical and predementia Alzheimer's disease. Neurobiol Aging. 2014;35(9):1973-81.
8. FDG-PET and amyloid-PET imaging: The diverging paths, (2014).
9. Shaffer JL, Petrella JR, Sheldon FC, Choudhury KR, Calhoun VD, Coleman RE, et al. Predicting cognitive decline in subjects at risk for Alzheimer disease by using combined cerebrospinal fluid, MR imaging, and PET biomarkers. Radiology. 2013;266(2):583-91.
10. Mosconi L, Tsui WH, Herholz K, Pupi A, Drzezga A, Lucignani G, et al. Multicenter standardized 18F-FDG PET diagnosis of mild cognitive impairment, Alzheimer's disease, and other dementias. Journal of nuclear medicine : official publication, Society of Nuclear Medicine. 2008;49(3):390-8.
11. Cerami C, Della Rosa PA, Magnani G, Santangelo R, Marcone A, Cappa SF, et al. Brain metabolic maps in Mild Cognitive Impairment predict heterogeneity of progression to dementia. NeuroImage Clinical. 2015;7:187-94.
12. Perani D, Cerami C, Caminiti SP, Santangelo R, Coppi E, Ferrari L, et al. Cross-validation of biomarkers for the early differential diagnosis and prognosis of dementia in a clinical setting. European journal of nuclear medicine and molecular imaging. 2016;43(3):499-508.
13. Nestor PJ, Altomare D, Festari C, Drzezga A, Rivolta J, Walker Z, et al. Clinical utility of FDG-PET for the differential diagnosis among the main forms of dementia. Eur J Nucl Med Mol Imaging. 2018;45(9):1509-25.
14. Collette F, Van der Linden M, Delrue G, Salmon E. Frontal hypometabolism does not explain inhibitory dysfunction in Alzheimer disease. Alzheimer Dis Assoc Disord. 2002;16(4):228-38.
15. Meyer F, Wehenkel M, Phillips C, Geurts P, Hustinx R, Bernard C, et al. Characterization of a temporoparietal junction subtype of Alzheimer's disease. Hum Brain Mapp. 2019;40(14):4279-86.
16. Teipel S, Grothe MJ, Alzheimer s Disease Neuroimaging I. Does posterior cingulate hypometabolism result from disconnection or local pathology across preclinical and clinical stages of Alzheimer's disease? Eur J Nucl Med Mol Imaging. 2016;43(3):526-36.
17. Crane PK, Carle A, Gibbons LE, Insel P, Mackin RS, Gross A, et al. Development and assessment of a composite score for memory in the Alzheimer's Disease Neuroimaging Initiative (ADNI). Brain Imaging Behav. 2012;6(4):502-16.
18. Gibbons LE, Carle AC, Mackin RS, Harvey D, Mukherjee S, Insel P, et al. A composite score for executive functioning, validated in Alzheimer's Disease Neuroimaging Initiative (ADNI) participants with baseline mild cognitive impairment. Brain Imaging Behav. 2012;6(4):517-27.
19. Landau SM, Thomas BA, Thurfjell L, Schmidt M, Margolin R, Mintun M, et al. Amyloid PET imaging in Alzheimer's disease: a comparison of three radiotracers. Eur J Nucl Med Mol Imaging. 2014;41(7):1398-407.
20. Hansson O, Seibyl J, Stomrud E, Zetterberg H, Trojanowski JQ, Bittner T, et al. CSF biomarkers of Alzheimer's disease concord with amyloid-beta PET and predict clinical progression: A study of fully automated immunoassays in BioFINDER and ADNI cohorts. Alzheimers Dement. 2018;14(11):1470-81.
21. Saykin AJ, Shen L, Foroud TM, Potkin SG, Swaminathan S, Kim S, et al. Alzheimer's Disease Neuroimaging Initiative biomarkers as quantitative phenotypes: Genetics core aims, progress, and plans. Alzheimers Dement. 2010;6(3):265-73.

22. Grothe MJ, Villeneuve S, Dyrba M, Bartres-Faz D, Wirth M, Alzheimer's Disease Neuroimaging I. Multimodal characterization of older APOE2 carriers reveals selective reduction of amyloid load. Neurology. 2017;88(6):569-76.
23. Wolf D, Bocchetta M, Preboske GM, Boccardi M, Grothe MJ, Alzheimer's Disease Neuroimaging I. Reference standard space hippocampus labels according to the European Alzheimer's Disease Consortium-Alzheimer's Disease Neuroimaging Initiative harmonized protocol: Utility in automated volumetry. Alzheimers Dement. 2017;13(8):893-902.
24. Desikan RS, Segonne F, Fischl B, Quinn BT, Dickerson BC, Blacker D, et al. An automated labeling system for subdividing the human cerebral cortex on MRI scans into gyral based regions of interest. Neuroimage. 2006;31(3):968-80.
25. Risacher SL, Anderson WH, Charil A, Castelluccio PF, Shcherbinin S, Saykin AJ, et al. Alzheimer disease brain atrophy subtypes are associated with cognition and rate of decline. Neurology. 2017;89(21):2176-86.
26. Schwarz C, Fletcher E, DeCarli C, Carmichael O. Fully-automated white matter hyperintensity detection with anatomical prior knowledge and without FLAIR. Inf Process Med Imaging. 2009;21:239-51.
27. DeCarli C, Fletcher E, Ramey V, Harvey D, Jagust WJ. Anatomical mapping of white matter hyperintensities (WMH): exploring the relationships between periventricular WMH, deep WMH, and total WMH burden. Stroke. 2005;36(1):50-5.
28. Lange C, Suppa P, Frings L, Brenner W, Spies L, Buchert R. Optimization of Statistical Single Subject Analysis of Brain FDG PET for the Prognosis of Mild Cognitive Impairment-to-Alzheimer's Disease Conversion. J Alzheimers Dis. 2016;49(4):945-59.
29. Matias-Guiu JA, Diaz-Alvarez J, Ayala JL, Risco-Martin JL, Moreno-Ramos T, Pytel V, et al. Clustering Analysis of FDG-PET Imaging in Primary Progressive Aphasia. Frontiers in aging neuroscience. 2018;10:230.
30. Noh Y, Jeon S, Lee JM, Seo SW, Kim GH, Cho H, et al. Anatomical heterogeneity of Alzheimer disease: based on cortical thickness on MRIs. Neurology. 2014;83(21):1936-44.
31. Davies DL, Bouldin DW. A cluster separation measure. IEEE Trans Pattern Anal Mach Intell. 1979;1(2):224-7.
32. Rousseeuw PJ. Silhouettes - a Graphical Aid to the Interpretation and Validation of Cluster-Analysis. Journal of Computational and Applied Mathematics. 1987;20:53-65.
33. Benjamini Y, Yekutieli D. The control of the false discovery rate in multiple testing under dependency. The Annals of Statistics. 2001;29(4):1165-88.
34. Teipel SJ, Dyrba M, Chiesa PA, Sakr F, Jelistratova I, Lista S, et al. In vivo staging of regional amyloid deposition predicts functional conversion in the preclinical and prodromal phases of Alzheimer's disease. Neurobiol Aging. 2020;93:98-108.
35. Ray NJ, Bradburn S, Murgatroyd C, Toseeb U, Mir P, Kountouriotis GK, et al. In vivo cholinergic basal forebrain atrophy predicts cognitive decline in de novo Parkinson's disease. Brain. 2018;141(1):165-76.
36. Mosconi L. Brain glucose metabolism in the early and specific diagnosis of Alzheimer's disease. FDG-PET studies in MCI and AD. Eur J Nucl Med Mol Imaging. 2005;32(4):486-510.
37. Poulakis K, Pereira JB, Mecocci P, Vellas B, Tsolaki M, Kloszewska I, et al. Heterogeneous patterns of brain atrophy in Alzheimer's disease. Neurobiol Aging. 2018;65:98-108.
38. Hwang J, Kim CM, Jeon S, Lee JM, Hong YJ, Roh JH, et al. Prediction of Alzheimer's disease pathophysiology based on cortical thickness patterns. Alzheimers Dement (Amst). 2016;2:58-67.

39. Klupp E, Grimmer T, Tahmasian M, Sorg C, Yakushev I, Yousefi BH, et al. Prefrontal hypometabolism in Alzheimer disease is related to longitudinal amyloid accumulation in remote brain regions. J Nucl Med. 2015;56(3):399-404.
40. La Joie R, Landeau B, Perrotin A, Bejanin A, Egret S, Pélerin A, et al. Intrinsic connectivity identifies the hippocampus as a main crossroad between Alzheimer's and semantic dementia-targeted networks. Neuron. 2014;81(6):1417-28.
41. Villain N, Fouquet M, Baron JC, Mezenge F, Landeau B, de La Sayette V, et al. Sequential relationships between grey matter and white matter atrophy and brain metabolic abnormalities in early Alzheimer's disease. Brain. 2010;133(11):3301-14.
42. Botha H, Mantyh WG, Murray ME, Knopman DS, Przybelski SA, Wiste HJ, et al. FDG-PET in tau-negative amnestic dementia resembles that of autopsy-proven hippocampal sclerosis. Brain : a journal of neurology. 2018;141(4):1201-17.
43. Ferreira D, Shams S, Cavallin L, Viitanen M, Martola J, Granberg T, et al. The contribution of small vessel disease to subtypes of Alzheimer's disease: a study on cerebrospinal fluid and imaging biomarkers. Neurobiology of aging. 2018;70:18-29.
44. Ossenkoppele R, Pijnenburg YA, Perry DC, Cohn-Sheehy BI, Scheltens NM, Vogel JW, et al. The behavioural/dysexecutive variant of Alzheimer's disease: clinical, neuroimaging and pathological features. Brain : a journal of neurology. 2015;138(Pt 9):2732-49.
45. Dong A, Toledo JB, Honnorat N, Doshi J, Varol E, Sotiras A, et al. Heterogeneity of neuroanatomical patterns in prodromal Alzheimer's disease: links to cognition, progression and biomarkers. Brain. 2017;140(3):735-47.
46. Young AL, Marinescu RV, Oxtoby NP, Bocchetta M, Yong K, Firth NC, et al. Uncovering the heterogeneity and temporal complexity of neurodegenerative diseases with Subtype and Stage Inference. Nat Commun. 2018;9(1):4273.

Supplemental Information

Additional file 1:

Supplementary table 1. Structures defined in the Harvard-Oxford atlas that were used to measure the composite cortical volume.

Supplementary table 2. Hazard ratios for progression of subtypes of patients with prodromal AD to dementia.

Supplementary table 3. Mixed effects regression models of longitudinal cognitive decline across subtypes in the prodromal AD group; “no hypometabolism” subtype as reference.

Supplementary table 4. Mixed effects regression models of longitudinal cognitive decline across subtypes in the prodromal AD group; “limbic-predominant” subtype as reference.

Supplementary table 5. Missing values (at baseline) for demographic, clinical and biomarker characteristics in the AD dementia and prodromal AD samples.

Supplementary Fig. 1. Determination of optimal clustering cutoff by objective criteria.

Supplementary Fig. 2. Hierarchical clustering dendrogram and hypometabolic FDG-PET patterns of resulting AD subtypes at higher cluster solutions.

Tables

Table 1 Demographic, clinical and biomarker characteristics of AD dementia subtypes at baseline.

	CN group	AD group, limbic-predominant (S1)	AD group, typical (S2)	AD group, cortical-predominant (S3)	P-value, Global comparison (S1, S2 and S3)	Pair-wise comparisons		
						S1 vs S2	S1 vs S3	S2 vs S3
Demographics								
n (%)	179	79 (44.6%)	86 (48.6%)	12 (6.8%)				
Age, years	73.8 (6.5)	75.4 (6.9)	73.2 (5.7)	68.0 (7.7)	0.007	0.149	0.015	0.088
Sex, female (%)	50%	49%	38%	50%	0.332			
Education, years	16.6 (2.5)	15.4 (3.1)	15.5 (2.6)	16.3 (2.6)	0.544			
Cognition								
MMSE	29.1 (1.2)	23.4 (1.9)	23.2 (2.2)	22.0 (2.2)	0.037	0.798	0.165	0.200
ADNI-MEM	1.04 (0.62)	-0.85 (0.55)	-0.90 (0.49)	-1.31 (0.44)	0.012	1	0.025	0.028
ADNI-EF	0.92 (0.83)	-0.65 (0.86)	-1.11 (0.89)	-1.73 (0.81)	< 0.001	0.002	< 0.001	0.043
ADNI-DIFF	0.13 (0.72)	-0.21 (0.69)	0.21 (0.85)	0.41 (0.74)	< 0.001	0.004	0.029	0.723
Visuospatial function	4.7 (0.6)	3.6 (1.3)	3.2 (1.5)	2.4 (1.4)	0.011	0.114	0.032	0.146
Language function	28.3 (2.1)	21.7 (5.9)	23.0 (5.5)	23.3 (6.2)	0.606	-	-	-
Biomarkers								
APOE ε4 (%)	28%	81%	79%	58%	0.222			
AV45-PET SUVR	1.11 (0.18)	1.43 (0.14)	1.47 (0.17)	1.4 (0.17)	0.145			
CSF Aβ, pg/ml	1392 (663)	598 (163)	585 (225)	629 (169)	0.686			
CSF t-tau, pg/ml	236 (92)	374 (143)	374 (154)	402 (124)	0.978			
CSF p-tau, pg/ml	22 (9)	38 (16)	37 (16)	39 (14)	0.881			
HV	4.97 (0.38)	4.05 (0.51)	4.1 (0.38)	4.46 (0.46)	0.09			
CTV	87.39 (6.28)	75.84 (6.95)	73.99 (6.23)	70.04 (5.88)	0.006	0.136	0.026	0.136
HV:CTV ratio	57.11	53.67 (7.57)	55.74	64.29	< 0.001	0.136	<	<

	(5.29)		(6.61)	(10.08)		0.001	0.001
WMH	6.1 (10.4)	8.0 (10.0)	5.8 (7.9)	8.1 (12.7)	0.262		

Values for variables are presented as percentages (for gender and APOE ε4 genotype) or means with standard deviation in parentheses. Missing values are excluded (for numbers of missing values per subtype see Supplementary table 5). In case of significant main effects, subtypes were compared with post-hoc pairwise t-tests with FDR correction. S1 = limbic-predominant subtype; S2 = typical subtype; S3 = cortical-predominant subtype. HV: hippocampal grey matter volume scaled to total intracranial volume. CTV: cortical composite grey matter volume scaled to total intracranial volume.

Table 2 Demographic, clinical and biomarker characteristics of prodromal AD subtypes at baseline.

	Prodromal AD group, no hypometabolism (S0)	Prodromal AD group, limbic-predominant (S1)	Prodromal AD group, typical (S2)	P-value, Global comparison (S0, S1 and S2)	Pair-wise comparisons		
					S0 vs S1	S0 vs S2	S1 vs S2
Demographics							
n (%)	57 (26.3%)	108 (49.8%)	49 (22.6%)				
Age, years	68.4 (6.6)	76.1 (5.7)	71.7 (6.2)	< 0.001	< 0.001	0.009	< 0.001
Sex, female (%)	60%	35%	41%	0.01	0.024	0.226	1
Education, years	16.2 (2.8)	15.7 (3.0)	16.4 (2.6)	0.344			
Cognition							
MMSE	28.2 (1.8)	27.6 (1.8)	27.3 (1.8)	0.053			
ADNI-MEM	0.57 (0.63)	0.05 (0.61)	-0.06 (0.65)	< 0.001	< 0.001	< 0.001	0.602
ADNI-EF	0.76 (0.91)	0.00 (0.77)	0.15 (1.01)	0.018	< 0.001	0.001	0.542
ADNI-DIFF	-0.19 (0.83)	0.05 (0.78)	-0.21 (0.77)	0.616			
Visuospatial function	4.5 (0.7)	4.4 (0.8)	4.3 (0.8)	0.565			
Language function	27.3 (2.6)	25.4 (3.9)	27.0 (3.4)	0.133			
Biomarkers							
APOE ε4 (%)	68%	62%	77%	0.163			
AV45-PET SUVR	1.31 (0.17)	1.39 (0.17)	1.43 (0.15)	0.004	0.015	0.002	0.238
CSF Aβ, pg/ml	921 (437)	736 (237)	672 (214)	0.002	< 0.001	< 0.001	0.417
CSF t-tau, pg/ml	315 (134)	337 (137)	357 (144)	0.123			
CSF p-tau, pg/ml	31 (15)	34 (16)	37 (16)	0.096			
HV	4.86 (0.45)	4.53 (0.51)	4.57 (0.41)	0.009	< 0.001	0.005	1
CTV	89.87 (5.45)	83.191 (6.48)	82.93 (5.35)	< 0.001	< 0.001	< 0.001	1
HV:CTV ratio	54.26 (6.07)	54.57 (6.27)	55.24 (5.56)	0.344			

WMH	4.9 (5.0)	11.3 (12.8)	6.8 (6.5)	0.172

Cortical-predominant subtype of prodromal AD group (n = 3) not included. Values for variables are presented as percentages (for gender and APOE ε4 genotype) or means with standard deviation in parentheses. Missing values are excluded (for numbers of missing values per subtype see Supplementary table 5). In case of significant main effects, subtypes were compared with post-hoc pairwise t-tests with FDR correction. S0 = no hypometabolism subtype; S1 = limbic-predominant subtype; S2 = typical subtype. HV: hippocampal grey matter volume scaled to total intracranial volume. CTV: cortical composite grey matter volume scaled to total intracranial volume.

Figures

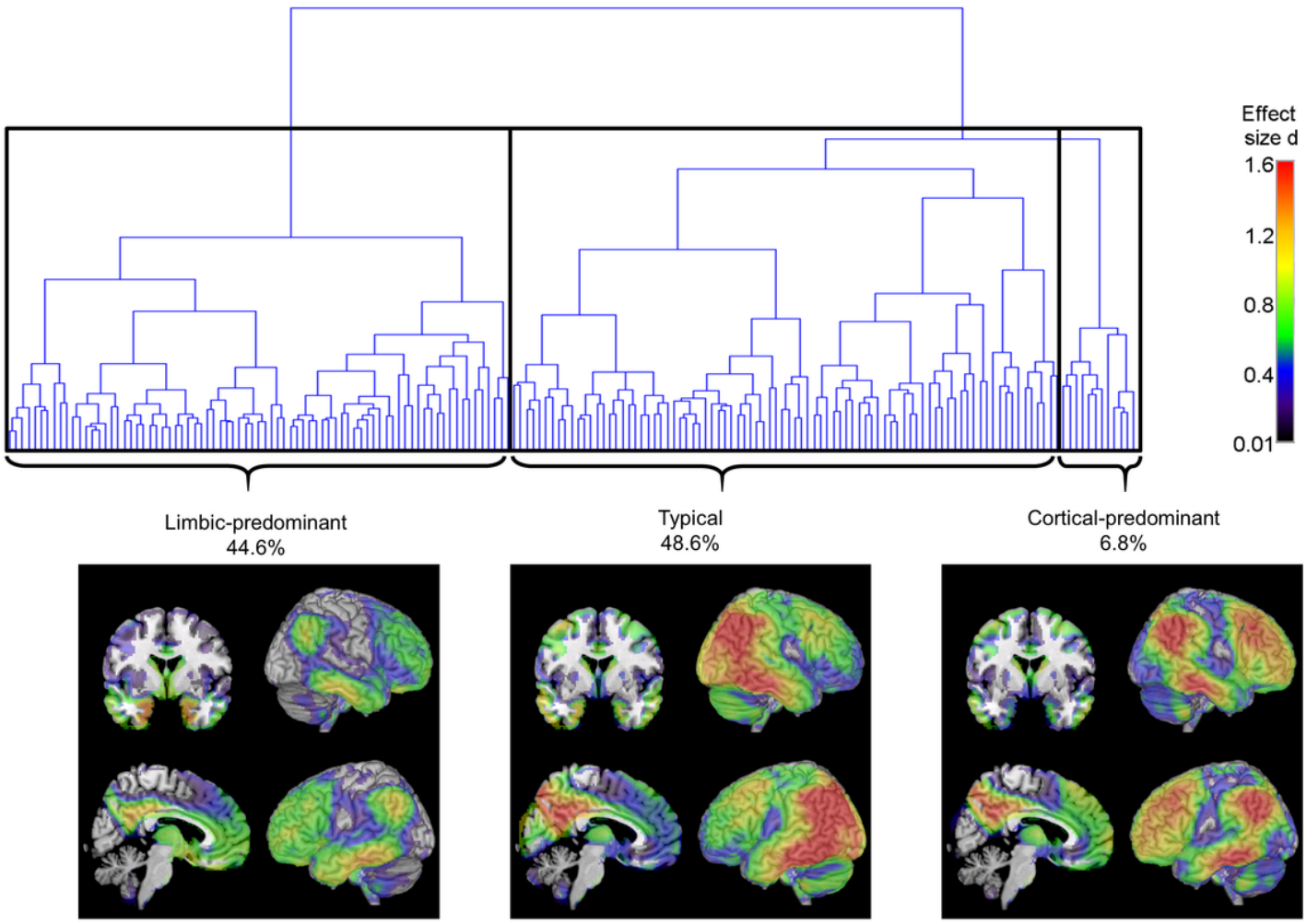

Figure 1

Hierarchical clustering dendrogram and hypometabolic FDG-PET patterns of identified AD subtypes. Dendrogram resulting from Ward's hierarchical clustering analysis of individual FDG-PET profiles of patients with AD dementia. Brain plots show voxel-wise hypometabolic patterns of the three identified AD subtypes as revealed by statistical comparison to the healthy control group. FDG-PET scans were scaled to the average pons signal prior to the group comparisons, and age, gender, and years of education were used as covariates. Statistical parametric maps of the group differences were converted into Cohen's d effect size maps to allow for a better comparison of the

patterns across the unevenly sized AD subgroups. Subtype patterns at higher clustering solutions are shown in Supplementary figure 2.

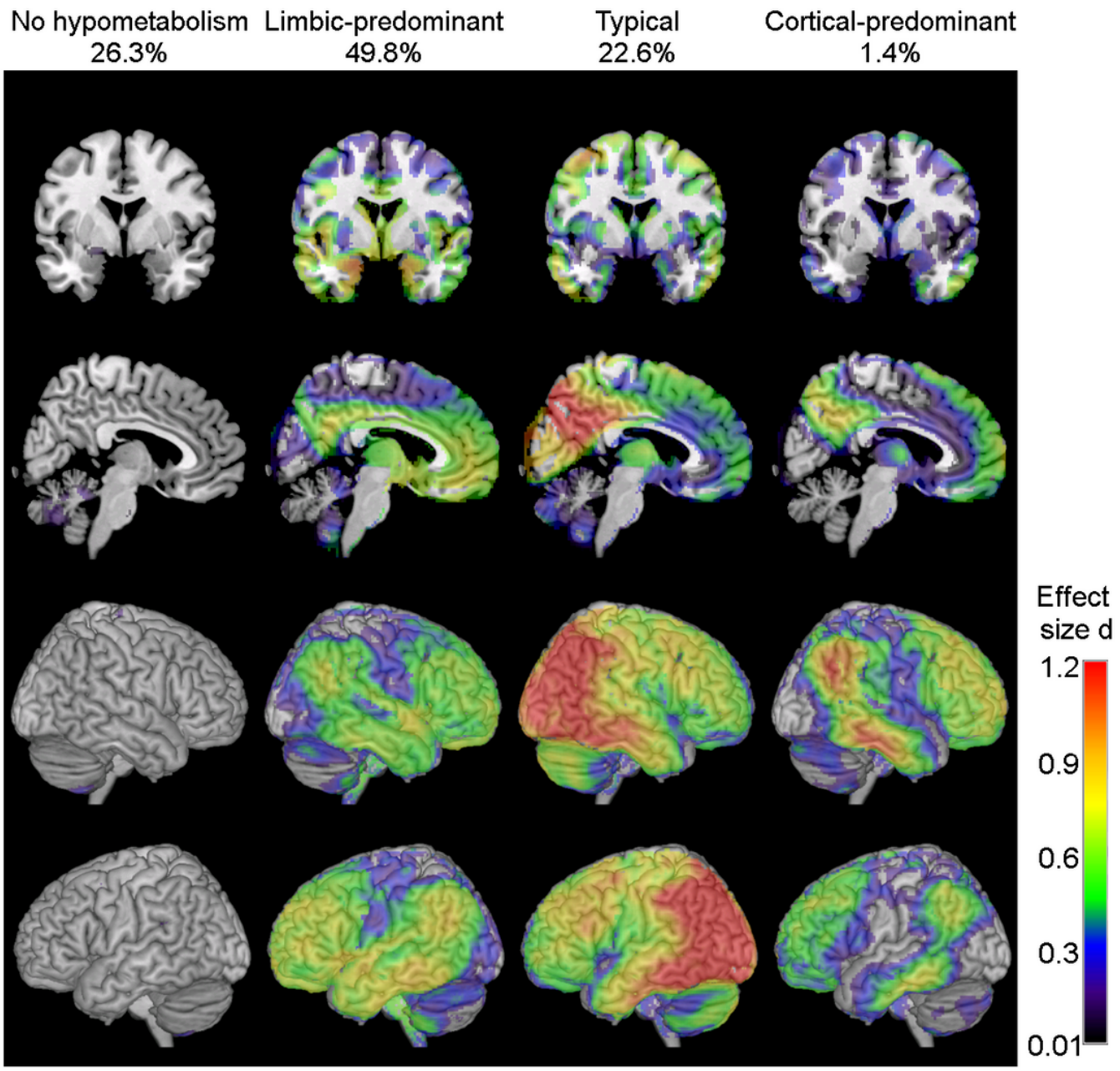

Figure 2

Hypometabolic FDG-PET patterns of subtypes of patients with prodromal AD Voxel-wise hypometabolic patterns of the four prodromal AD subtypes as compared to the healthy control group. FDG-PET scans were scaled to the average pons signal prior to analysis, and age, gender, and years of education were used as covariates. Statistical parametric maps of the group differences were converted into Cohen's d effect size maps to allow for a better comparison of the patterns across the unevenly sized subgroups.

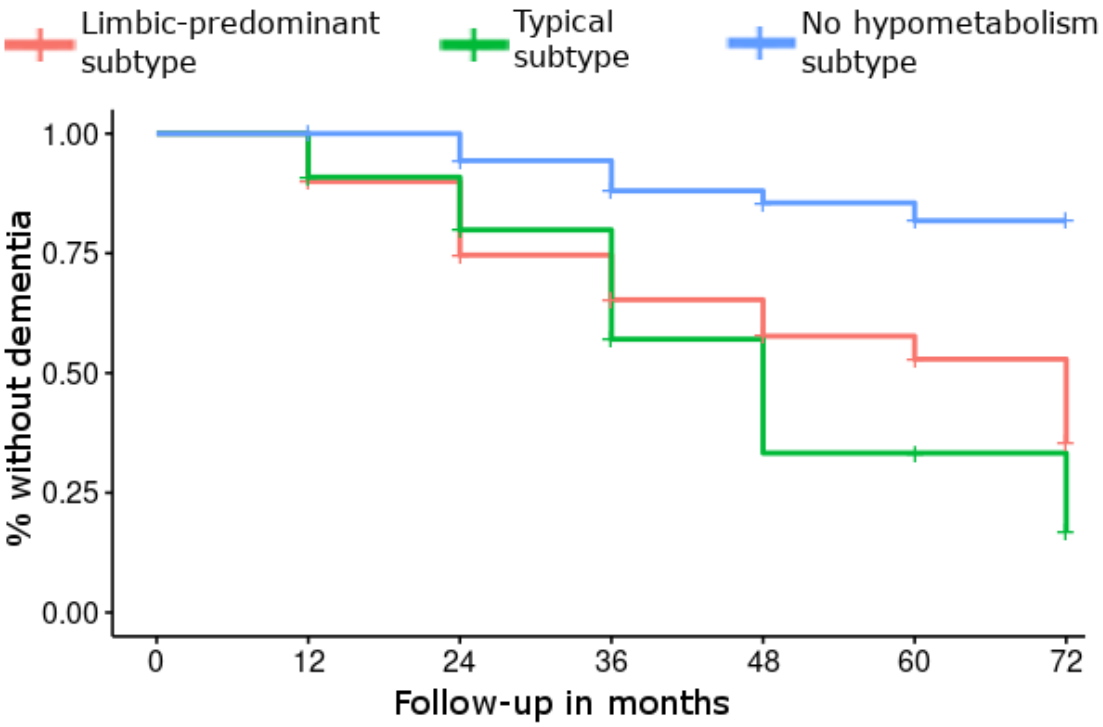

Figure 3

Kaplan-Meier curves of time to progression to dementia across subtypes in the prodromal AD group. Kaplan-Meier survival curves indicate proportions of participants within the three prodromal AD subtypes progressing to dementia, operationalized as a change in CDR score from 0.5 to ≥ 1. Patients who did not progress to dementia within the observation period or did not have follow-up CDR scores were censored.

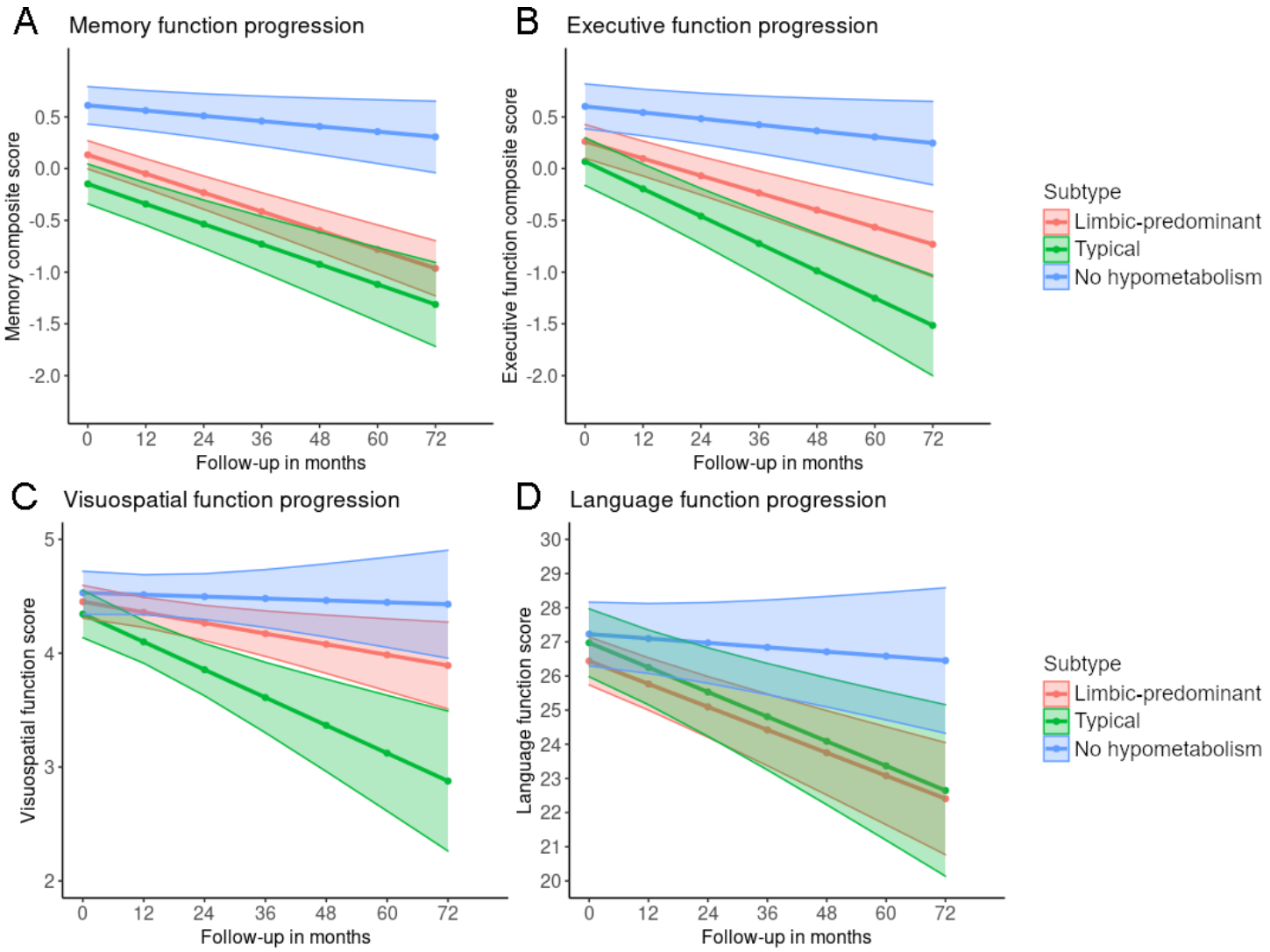

Figure 4

Longitudinal cognitive trajectories of subtypes of patients with prodromal AD. Predicted values of domain-specific cognitive scores were obtained from mixed effects regression models which included age, gender, and years of education as covariates, as well as random intercepts and slopes for participants to account for multiple measurements. (A) Memory function progression. (B) Executive function progression. (C) Visuospatial function progression. (D) Language function progression. Ribbons around regression lines represent 95% confidence intervals for the fitted values.

Supplementary Files

This is a list of supplementary files associated with this preprint. Click to download.

- Supplementaryinformation.docx